Simulation of Electromagnetic Modes in a Rectangular PEC Cavity Using the FDTD Method

Erich Wanzek

ELEC 4333, University of Colorado Denver

(Dated: April 8, 2021)

I. PROJECT DESCRIPTION

The objective of this project was to develop a numerical routine in software that performs a FDTD solution of Maxwell's equations in three dimensions, specifically in a rectangular cavity with perfect electrical conducting boundaries (PEC). The software was validated for the case of a cubic cavity of varying node density.

The software developed in this project is capable of simulating Maxwell's equations using second-order accurate central difference approximations of Maxwell's equations, specifically Ampere's law and Faraday's law governing electromagnetic field transients. In this project the FDTD method is employed for the simplest case in three dimensions, which is a rectangular cavity bounded with PECs. In this FDTD code, the PEC rectangular cavity is excited by a current source with a differentiated Gaussian pulse signature. The gaussian pulse allows for excitation of all frequencies contained within the bandwidth of the Fourier spectrum of the gaussian pulse. The injected electric field Gaussian pulse will then excite the resonant modes of the cavity being analyzed. By recording the electric field along a specified mesh edge, the transient electric field can then be sampled over the duration of the simulation time. This transient electric field signal can subsequently be Fourier transformed by use of the FFT algorithm to observe the resonant modes of the PEC cavity that were excited by the differentiated gaussian pulse.

The theory of the FDTD simulation of Maxwell's equations in three dimensions will be discussed in the next section. In the following section the top-level code design of the FDTD software will be briefly discussed, and finally the FDTD software will be validated by running a series of FDTD simulations of a cubic meter PEC cavity with different amounts of nodes for each case. Validation will be performed by comparing the the resonant frequencies extracted from the FDTD simulation with the analytical solutions of the resonant frequencies

in a rectangular PEC cavity. Validation will be quantitatively analyzed by calculating the relative error between the FDTD numerically computed resonant frequency and the analytical resonant frequency of a specified mode as a function of the FDTD grid size. This will demonstrate the 2nd order accuracy of the numerical solution as the relative error decreases by a factor of 2 for each decade increase in the amount of nodes along each dimension.

II. THEORY

In order to numerically solve Maxwell's equations in three dimensions, the finite difference time domain (FDTD) method is employed. A brief overview of the theory of the FDTD update equations used for modeling Maxwell equations and the source excitations are covered in this section.

Maxwell's equations consist of four equations which are listed here. The first equation is Gauss's Law:

$$\nabla \cdot \overrightarrow{D} = \rho \tag{1}$$

The second equation is Gauss's law for magnetic charges

$$\nabla \cdot \overrightarrow{B} = \rho^* \tag{2}$$

The third equation is Faraday's Law. Faraday's law is given by the partial differential vector equation:

$$\frac{\partial \overrightarrow{B}}{\partial t} = -\nabla \times \overrightarrow{E} - \overrightarrow{M} \tag{3}$$

The fourth equation is Ampere's Law. Amperes law is given by the partial differential vector equation:

$$\frac{\partial \overrightarrow{D}}{\partial t} = \nabla \times \overrightarrow{H} - \overrightarrow{J} \tag{4}$$

Additionally, the material constitutive relations encode the relation between electric and magnetic flux densities and the electric and magnetic fields intensities by the electrical permittivity and the magnetic permeability coefficients. In linear isotropic media, these relations are linear and have the same permeability and permittivity throughout the whole media. These relations are given by:

$$\overrightarrow{D} = \varepsilon \overrightarrow{E} = \varepsilon_0 \varepsilon_r \overrightarrow{E} \tag{5}$$

$$\overrightarrow{B} = \mu\overrightarrow{H} = \mu_0\mu_r\overrightarrow{H} \tag{6}$$

The discrete version of Maxwell's equations, specifically Ampere's law and Faraday's law, can be derived from approximating the 1st order time derivatives and 1st order space derivatives of the curl operators with a 2nd order accurate central difference approximation. After substituting the derivatives of Ampere's Law and Faraday's law with second order accurate central difference approximations, and rearranging terms so that the field components at a later time are given explicitly by updating the past field component, the FDTD update equations are formulated. The FDTD update equations for the electric and magnetic field vector components are listed below.

$$E^{n+\frac{1}{2}}_{x_{i+\frac{1}{2},j,k}} = E^{n-\frac{1}{2}}_{x_{i+\frac{1}{2},j,k}} + \frac{\Delta t}{\varepsilon}\left[\left(\frac{H^n_{z_{i+\frac{1}{2},j+\frac{1}{2},k}} - H^n_{z_{i+\frac{1}{2},j-\frac{1}{2},k}}}{\Delta y}\right) - \left(\frac{H^n_{y_{i+\frac{1}{2},j,k+\frac{1}{2}}} - H^n_{y_{i+\frac{1}{2},j,k-\frac{1}{2},k}}}{\Delta z}\right) - J^n_{x_{i+\frac{1}{2},j,k}}\right] \tag{7}$$

$$E^{n+\frac{1}{2}}_{y_{i,j+\frac{1}{2},k}} = E^{n-\frac{1}{2}}_{y_{i,j+\frac{1}{2},k}} + \frac{\Delta t}{\varepsilon}\left[\left(\frac{H^n_{x_{i,j+\frac{1}{2},k+\frac{1}{2}}} - H^n_{x_{i,j+\frac{1}{2},k-\frac{1}{2}}}}{\Delta z}\right) - \left(\frac{H^n_{z_{i+\frac{1}{2},j+\frac{1}{2},k}} - H^n_{z_{i-\frac{1}{2},j+\frac{1}{2},k}}}{\Delta x}\right) - J^n_{y_{i,j+\frac{1}{2},k}}\right] \tag{8}$$

$$E^{n+\frac{1}{2}}_{z_{i,j,k+\frac{1}{2}}} = E^{n-\frac{1}{2}}_{z_{i,j,k+\frac{1}{2}}} + \frac{\Delta t}{\varepsilon}\left[\left(\frac{H^n_{y_{i+\frac{1}{2},j,k+\frac{1}{2}}} - H^n_{y_{i-\frac{1}{2},j,k+\frac{1}{2}}}}{\Delta x}\right) - \left(\frac{H^n_{x_{i,j+\frac{1}{2},k+\frac{1}{2}}} - H^n_{x_{i,j-\frac{1}{2},k+\frac{1}{2}}}}{\Delta y}\right) - J^n_{z_{i,j,k+\frac{1}{2}}}\right] \tag{9}$$

$$H^{n+1}_{x_{i,j+\frac{1}{2},k+\frac{1}{2}}} = H^n_{x_{i,j+\frac{1}{2},k+\frac{1}{2}}} + \frac{\Delta t}{\mu}\left[\left(\frac{E^{n+\frac{1}{2}}_{y_{i,j+\frac{1}{2},k+1}} - E^{n+\frac{1}{2}}_{y_{i,j+\frac{1}{2},k}}}{\Delta z}\right) - \left(\frac{E^{n+\frac{1}{2}}_{z_{i,j+1,k+\frac{1}{2}}} - E^{n+\frac{1}{2}}_{z_{i,j,k+\frac{1}{2}}}}{\Delta y}\right) - M^{n+\frac{1}{2}}_{x_{i,j+\frac{1}{2},k+\frac{1}{2}}}\right] \tag{10}$$

$$H^{n+1}_{y_{i+\frac{1}{2},j,k+\frac{1}{2}}} = H^n_{y_{i+\frac{1}{2},j,k+\frac{1}{2}}} + \frac{\Delta t}{\mu}\left[\left(\frac{E^{n+\frac{1}{2}}_{z_{i+1,j,k+\frac{1}{2}}} - E^{n+\frac{1}{2}}_{z_{i,j,k+\frac{1}{2}}}}{\Delta x}\right) - \left(\frac{E^{n+\frac{1}{2}}_{x_{i+\frac{1}{2},j,k+1}} - E^{n+\frac{1}{2}}_{x_{i+\frac{1}{2},j,k}}}{\Delta z}\right) - M^{n+\frac{1}{2}}_{y_{i+\frac{1}{2},j,k+\frac{1}{2}}}\right] \tag{11}$$

$$H^{n+1}_{z_{i+\frac{1}{2},j+\frac{1}{2},k}} = H^{n}_{z_{i+\frac{1}{2},j+\frac{1}{2},k}} + \frac{\Delta t}{\mu}\left[\left(\frac{E^{n+\frac{1}{2}}_{x_{i+\frac{1}{2},j+1,k}} - E^{n+\frac{1}{2}}_{x_{i+\frac{1}{2},j,k}}}{\Delta y}\right) - \left(\frac{E^{n+\frac{1}{2}}_{y_{i+1,j+\frac{1}{2},k}} - E^{n+\frac{1}{2}}_{y_{i,j+\frac{1}{2},k}}}{\Delta x}\right) - M^{n+\frac{1}{2}}_{z_{i+\frac{1}{2},j+\frac{1}{2},k}}\right]$$

(12)

In order for the numerical solution of the FDTD simulation to remain numerically stable the Courant-Fredrichs-Lewy stability limit condition must be satisfied. This limit will restrict the size of the time step given the chosen size of the spatial dimension steps and the CFLN number. The stability condition is given by equation 13.

$$\Delta t = \frac{1}{c_{max}} \frac{CFLN}{\sqrt{\frac{1}{\Delta x^2} + \frac{1}{\Delta y^2} + \frac{1}{\Delta z^2}}} \tag{13}$$

In the case of the simulations in this project a CFL number of 0.99 was used and the spatial step sizes were determined from the cavity dimensions and the number of nodes along each cavity dimension. In this project, the rectangular cavity will be bounded by perfect electrical conductor(PEC) boundaries. In a PEC the electric and magnetic fields within the PEC must be equal to zero. Thus the tangent electric field components will be equal to zeros as described by equation 14.

$$\widehat{n} \times \overrightarrow{E_1}\Big|_{S_{PEC}} = 0 \tag{14}$$

The electric flux density normal to the PEC surface will be equal to the induced electric charge density induced on the PEC surface as shown in equation 15.

$$\widehat{n} \times \overrightarrow{D_1}\Big|_{S_{PEC}} = \rho_s \tag{15}$$

Likewise, the magnetic field components perpendicular to the surface will be equal to the induced electric current surface density on the PEC surface as shown in equation 16

$$\widehat{n} \times \overrightarrow{H_1}\Big|_{S_{PEC}} = \overrightarrow{J_s} \tag{16}$$

The magnetic flux density normal to the PEC surface will be equal to zero as shown in equation 17.

$$\widehat{n} \times \overrightarrow{B_1}\Big|_{S_{PEC}} = 0 \tag{17}$$

For the implementation of PEC boundary conditions for the FDTD update equations, no update is performed on the electric field along the boundaries. The fields are instead initialized to zero and remain zero for the whole simulation duration since the electric and magnetic fields within PEC must be equal to zero.

III. CODE IMPLEMENTATION

In this section a brief overview of the implementation and top level design of the software that performs the 3D FDTD simulation of Maxwell's equations code is presented. The code first reads in all the physical data and simulation data required to perform the FDTD simulation by reading in a user edited text file. Next, in the setup FDTD function, all physical constants, material parameters and update equation coefficients are precalculated and the electric and magnetic field vector component node arrays are allocated memory and initialized to zero. After all parameters and data arrays are initialized, the FDTD update procedure commences. This procedure consists of a for loop that increments from the first time step to the last time step, where at each time step, the following array updating operator functions are executed in the order as now presented: the main electric field update, electric field source injection, main magnetic field update, and the save field data function.

The main electric field update function consists of a series of three nested for loops which update the electric field vector components at each node in the simulation volume, excluding the PEC boundaries. The update equations for the electric field updates are equations 7-9. Generally, for update of the fields on the boundaries, a separate update must be used to update the tangential electric fields on the exterior boundaries but for this project, this function will basically do nothing, leaving the tangential electric fields with a zero value throughout the simulation because the boundaries are PEC boundaries. The discrete electric field update equations used in the main electric field update are the same as equations 7-9 after translating from half indexing to integer indexing which is more suitable and standard in computer programming. The electric field update equations are listed below:

$$E_x(i,j,k) = E_x(i,j,k) + \frac{\Delta t}{\varepsilon}\left[\frac{1}{\Delta y}(H_z(i,j,k) - H_z(i,j-1,k)) - \frac{1}{\Delta z}(H_y(i,j,k) - H_y(i,j,k-1))\right] \tag{18}$$

$$E_y(i,j,k) = E_y(i,j,k) + \frac{\Delta t}{\varepsilon}\left[\frac{1}{\Delta z}(H_x(i,j,k) - H_x(i,j,k-1)) - \frac{1}{\Delta x}(H_z(i,j,k) - H_y(i-1,j,k))\right] \tag{19}$$

$$E_z(i,j,k) = E_z(i,j,k) + \frac{\Delta t}{\varepsilon}\left[\frac{1}{\Delta x}(H_y(i,j,k) - H_x(i-1,j,k)) - \frac{1}{\Delta y}(H_x(i,j,k) - H_y(i,j-1,k))\right] \tag{20}$$

The main magnetic field update function, in dual manor to the electric field update function, consists of a series of three nested for loops which update the magnetic field vector components at each node in the simulation volume. The update equations for the electric field are equations 10-12. The discrete electric field update equations used in the main magnetic field update function are the same as equations 10-12 after translating from half indexing to integer indexing. The magnetic field update equations are listed below:

$$H_x(i,j,k) = H_x(i,j,k) + \frac{\Delta t}{\mu}\left[\frac{1}{\Delta z}(E_y(i,j,k+1) - E_y(i,j,k)) - \frac{1}{\Delta y}(E_z(i,j+1,k) - E_z(i,j,k))\right] \tag{21}$$

$$H_y(i,j,k) = H_y(i,j,k) + \frac{\Delta t}{\mu}\left[\frac{1}{\Delta x}(E_z(i+1,j,k) - E_z(i,j,k)) - \frac{1}{\Delta z}(E_x(i,j,k+1) - E_x(i,j,k))\right] \tag{22}$$

$$H_z(i,j,k) = H_z(i,j,k) + \frac{\Delta t}{\mu}\left[\frac{1}{\Delta y}(E_x(i,j+1,k) - E_x(i,j,k)) - \frac{1}{\Delta x}(E_y(i+1,j,k) - E_y(i,j,k))\right] \tag{23}$$

Once the FDTD algorithm is complete, the post processing function is called. This function calls other functions which perform a calculation of the analytical modes of the theoretical PEC cavity, the FFT algorithm to compute the frequency spectrum, error calculations, and produce plots of the transient fields and field spectrums.

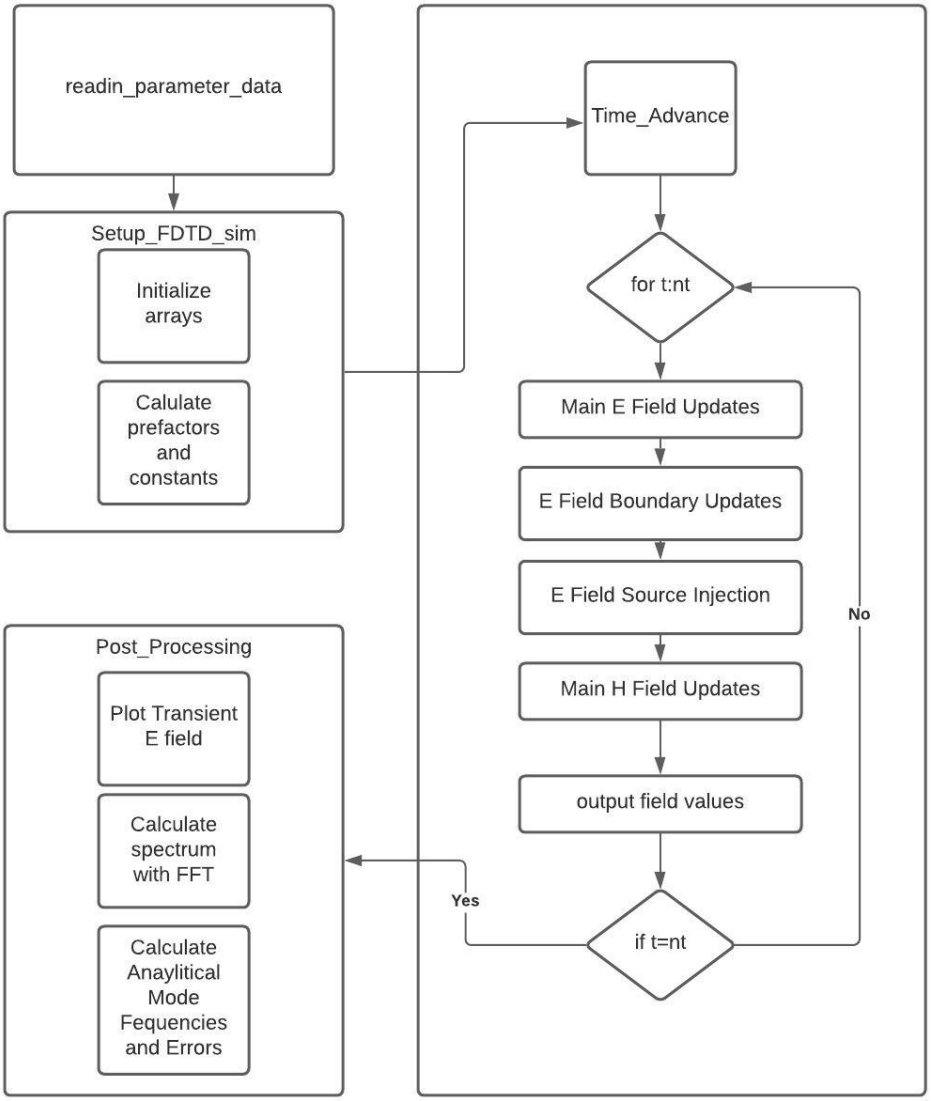

FIG. 1: Block Diagram of the top level functional design of the FDTD python script

IV. VALIDATING CASE STUDIES

In this section, simulations involving the computation of the resonant modes of the PEC cubic cavity performed with the FDTD software are compared against the analytical resonant modes to serve as proof of validation of the 3D FDTD model of Maxwell's equations implemented in the software.

A. Case Study i: 125 cell simulation, Nx=Ny=Nz=6

The first validation case study performed was a simulation of a cubic PEC cavity with length, width and height dimensions of one meter. The number of nodes was set equally to six in all three dimensions so that the FDTD simulation volume consisted of 125 cells. In this first simulation, the PEC cavity was excited by electric field injection via a current source occurring in the current density term of Maxwell-Ampere equation for the main electric field update. The source was injected along the edge bounded by the nodes $(i^1_{src}, j^1_{src}, k^1_{src}) = (2, 2, 2)$ and $(i^2_{src}, j^2_{src}, k^2_{src}) = (2, 2, 3)$. The electric field was probed and sampled by recording the z-component directed total electric field within the volume bounded by the nodes $(i^1_{fld}, j^1_{fld}, k^1_{fld}) = (4, 4, 4)$ and $(i^2_{fld}, j^2_{fld}, k^2_{fld}) = (4, 4, 5)$. The source signature was a differentiated Gaussian pulse with a half pulse width t_w=1ns to allow for a half bandwidth excitation off 300 Mhz to excite modes up to 600 MHz in the cavity. The pulse was set to have a time delay of $5t_w$.

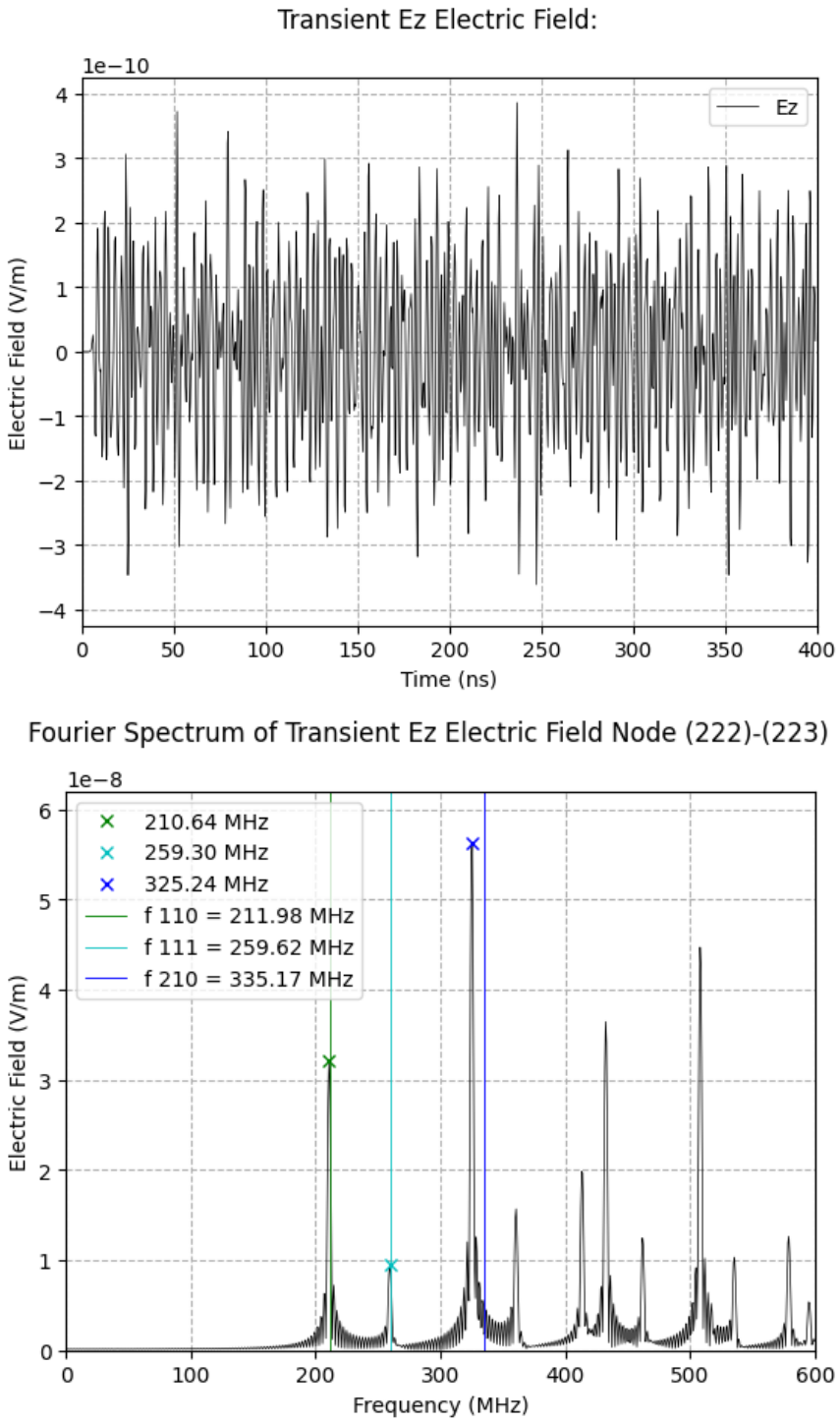

FIG. 2: Plots of the transient Ez field and its frequency spectrum at the edge between the specified nodes, for the case of N=6 in all three dimensions. X designates the computed frequency peaks of the resonant modes of the FDTD simulation, and the vertical lines represent the analytical mode frequencies. The first three lowest modes (f 110, f 210, f 211), were computed from the FDTD simulation.

As demonstrated in the plot in FIG 2, the results of this case study simulation show that the computed frequencies of the first three resonant modes of the PEC cavity correspond to the calculated analytical modes with slightly increasing error with increasing mode frequency. This correspondence of the computed mode frequencies from the FDTD simulation with the analytical modes verify that the FDTD simulation is simulating the correct behaviour as predicted by electromagnetic theory.

B. Case Study ii, 1000 cell simulation, Nx=Ny=Nz=11

The second validation case study performed was a simulation of a cubic PEC cavity with length, width and height dimensions of one meter. The number of nodes was set equally to 11 in all three dimensions so that the FDTD simulation volume consisted of 1000 cells. Just like the first case simulation, the PEC cavity was excited by electric field injection via a current source occurring in the current density term of Maxwell-Ampere equation for the main electric field update. The source was injected within the volume bounded by the nodes $(i^1_{src}, j^1_{src}, k^1_{src}) = (4, 4, 4)$ and $(i^2_{src}, j^2_{src}, k^2_{src}) = (4, 4, 6)$. The electric field was probed and sampled by recording the z-component directed total electric field within the volume bounded by the nodes $(i^1_{fld}, j^1_{fld}, k^1_{fld}) = (8, 8, 8)$ and $(i^2_{fld}, j^2_{fld}, k^2_{fld}) = (8, 8, 9)$. The source signature was a differentiated Gaussian pulse with a half pulse width t_w=1ns to allow for a half bandwidth excitation off 300 Mhz to excite modes up to 600 MHz in the cavity. The pulse was set to have a time delay of $5t_w$.

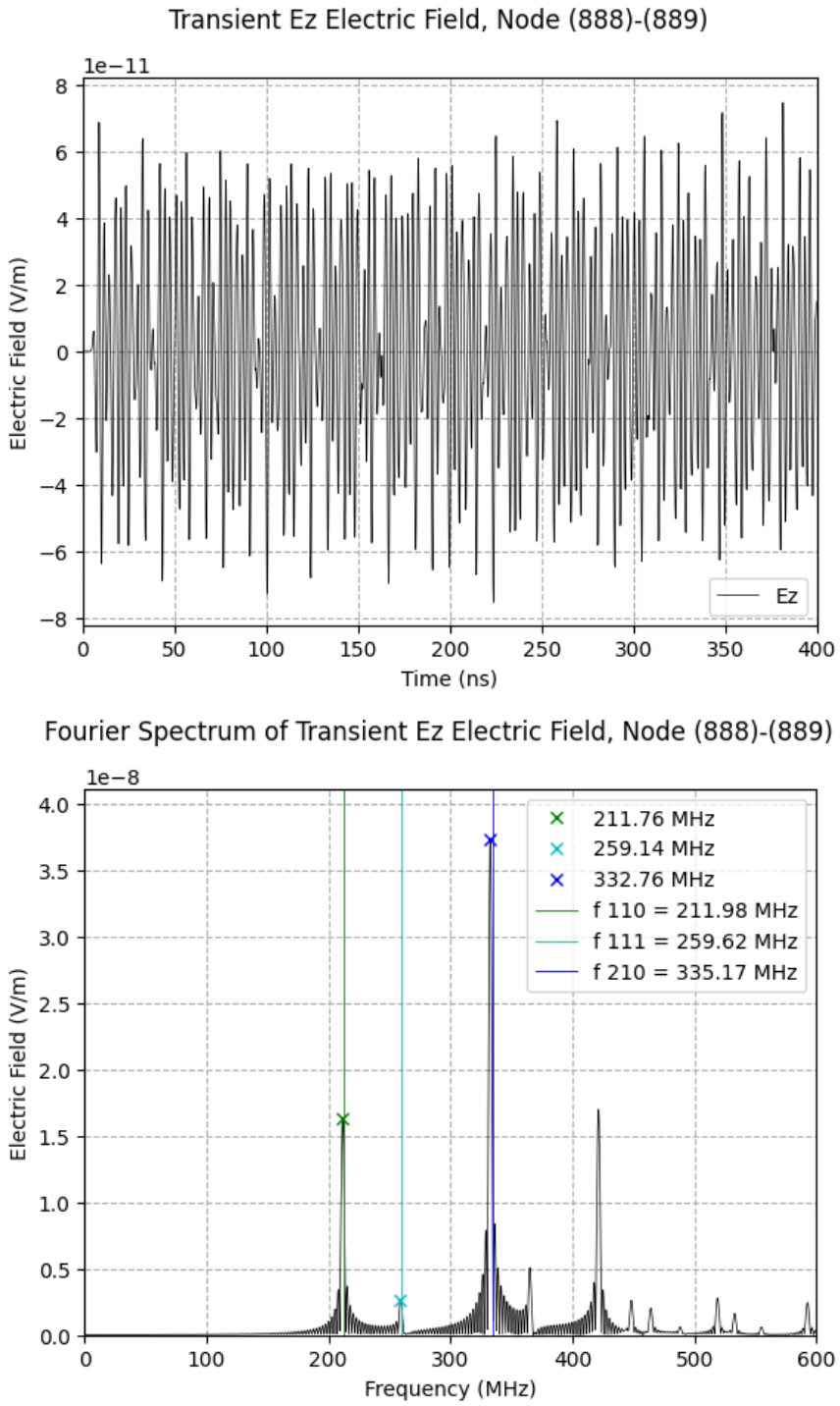

FIG. 3: Plots of the transient Ez field and its frequency spectrum at the edge between the specified nodes, for the case of N=11 in all three dimensions. Computed frequency peaks of the resonant modes of the FDTD simulation are marked with a X, and the vertical lines represent the analytical mode frequencies. The first three lowest modes (f 110, f 210, f 211) were computed from the FDTD simulation.

As demonstrated in the plot in FIG 3, the results of this case study simulation show that the computed frequencies of the first three resonant modes of the PEC cavity correspond to the calculated analytical modes with slightly increasing error with increasing mode frequency. The relative error between the computed modes and the analytical modes was also observed to improve in comparison to the previous case of the 125 cell simulation.

C. Case Study iii: 8,000 cell simulation, Nx=Ny=Nz=21

The third validation case study performed was a simulation of a cubic PEC cavity with length, width and height dimensions of one meter. The number of nodes was set equally to 21 in all three dimensions so that the FDTD simulation volume consisted of 8000 cells. Just like the preceding case simulation, the PEC cavity was excited by electric field injection via a current source occurring in the current density term of Maxwell-Ampere equation for the main electric field update. The source was injected within the volume bounded by the nodes $(i^1_{src}, j^1_{src}, k^1_{src}) = (8, 8, 8)$ and $(i^2_{src}, j^2_{src}, k^2_{src}) = (8, 8, 12)$. The electric field was probed and sampled by recording the z-component directed total electric field within the volume bounded by the nodes $(i^1_{fld}, j^1_{fld}, k^1_{fld}) = (16, 16, 16)$ and $(i^2_{fld}, j^2_{fld}, k^2_{fld}) = (16, 16, 17)$. The source signature was a differentiated Gaussian pulse with a half pulse width t_w=1ns to allow for a half bandwidth excitation off 300Mhz to excite modes up to 600 MHz in the cavity. The pulse was set to have a time delay of $5t_w$.

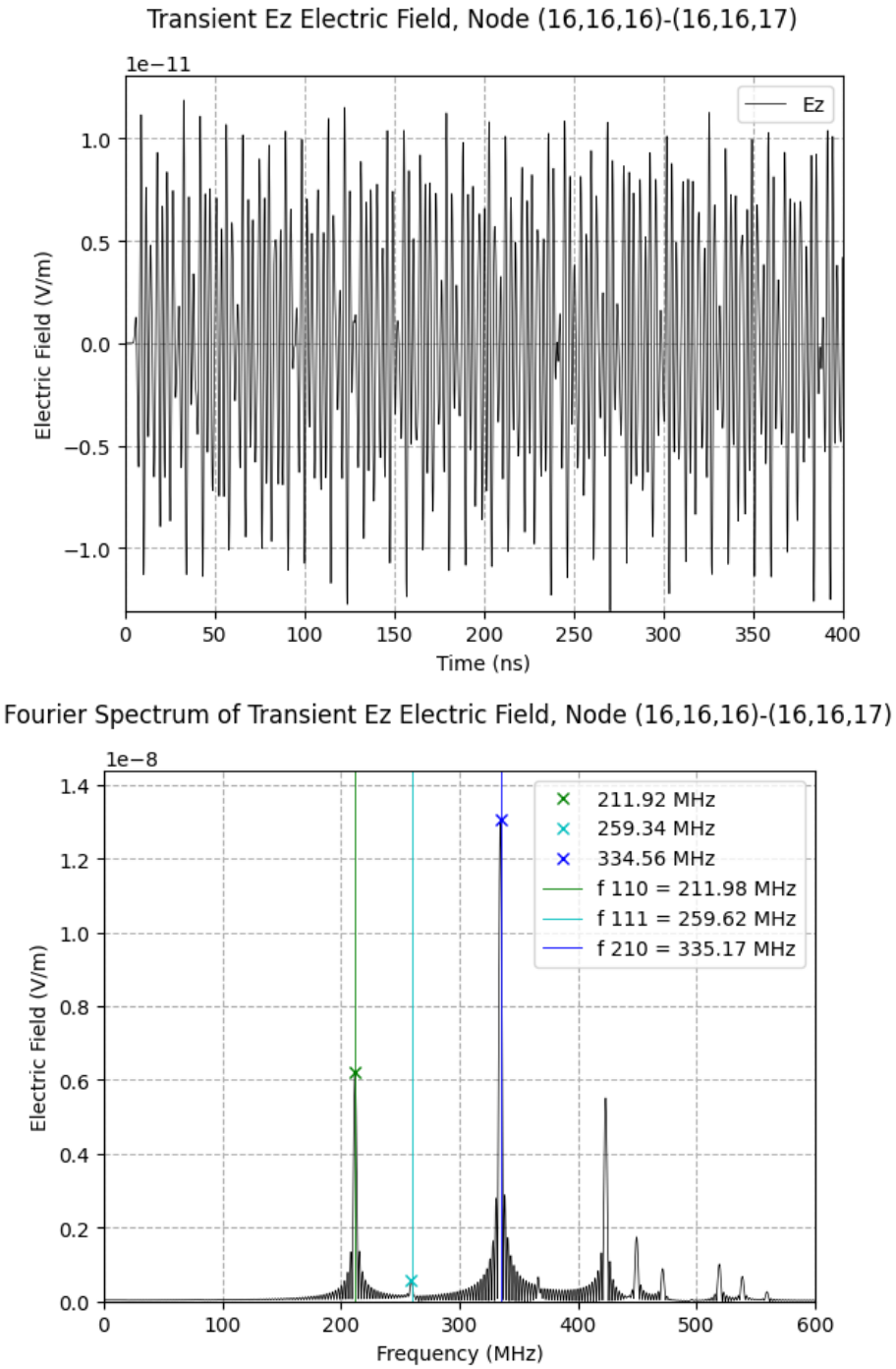

FIG. 4: Plots of the transient Ez field and its frequency spectrum at the edge between the specified nodes, for the case of N=21 in all three dimensions. Computed frequency peaks of the resonant modes of the FDTD simulation are marked with a X, and the vertical lines represent the analytical mode frequencies. The first three lowest modes (f 110, f 210, f 211) were computed from the FDTD simulation.

As demonstrated in the plot in FIG 4, the results of this case study simulation show that the computed frequencies of the first three resonant modes of the PEC cavity corresponded to the calculated analytical modes with a very small increase in error with increasing mode frequency. The relative error between the computed modes and the analytical modes were also observed to be smaller than the relative error in the previous 1000 cell simulation.

D. Validation of 2nd order Accuracy

In this section, the 2nd order accuracy of the FDTD simulation will be demonstrated by comparing the relative error between the numerically computed and analytical mode frequencies for the test simulations with different numbers of nodes.

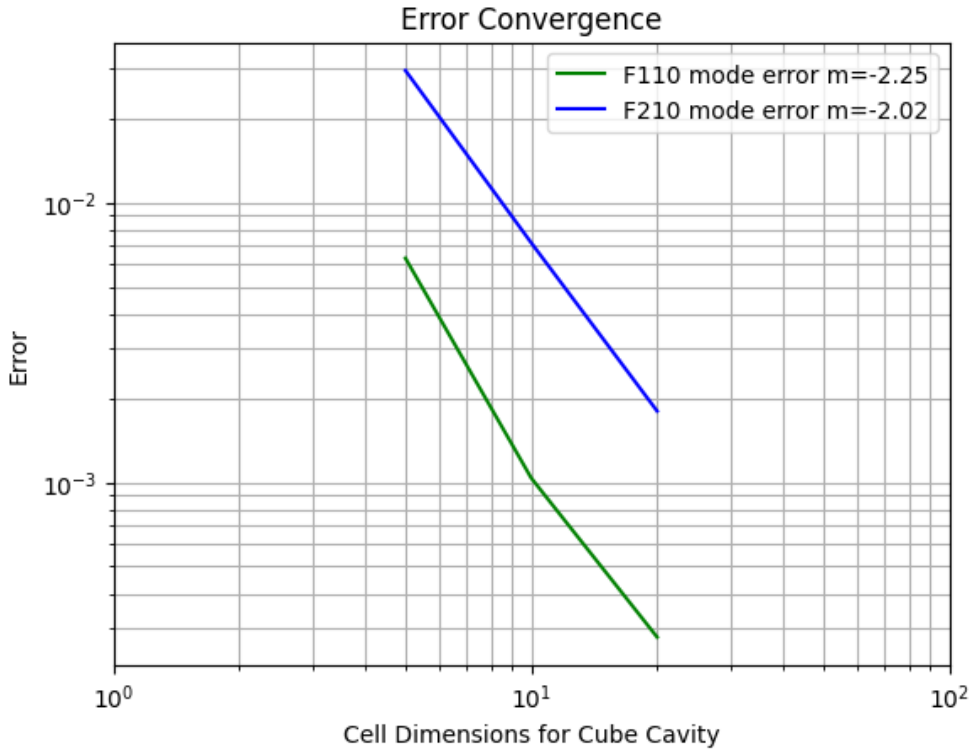

FIG. 5: This is the Log-Log plot of the relative error vs cell dimensions of the cavity. Error plots are shown for the F110 and F210 modes. m specifies the slope of the error plot.

The log-log error vs cell number plot of FIG 5. demonstrates 2nd order convergence of relative error between the analytical resonant modes and the numerically computed modes from the FDTD simulation. This 2nd order convergence is demonstrated by observation that

the approximate slope of the error convergence for the f110 and f210 modes has a slope of -2. This means that the relative error is decreasing by a factor of two for every decade increase in the number of cells in the FDTD simulation. This 2nd order decrease in relative error per decade increase of the number of cell dimensions in each dimension is attributed to the 2nd order accurate discrete approximation used by substitution of the time derivatives and spatial derivatives of the curl operators in Maxwell's equations with the 2nd order accurate central difference approximation.

V. SUMMARY

A code that performed a FDTD simulation of Maxwell's equations in a three dimensional rectangular PEC cavity was successfully developed in this project. The FDTD method used the 2nd order accurate central difference approximations for the equations. The code was validated by performing simulations of electromagnetic fields in a PEC cavity excited by a differentiated gaussian pulse and comparing the computed mode frequencies to the analytical mode frequencies. By observing the affect of increasing the nodes on the relative error of the computed mode frequencies and analytical mode frequencies, 2nd order accuracy of the numerical FDTD routine was demonstrated.